Transactions on Engineering and Computing Sciences - Vol. 13, No. 01
Publication Date: February 25, 2025
DOI:10.14738/tmlai.1301.18300.
Koueni, T. C. A. (2025). Numerical Modeling of Temperature and Pressure Fields in an Enclosure with Two Openings in Natural Convection. Transactions on Engineering and Computing Sciences, 13(01). 124-146.

Numerical Modeling of Temperature and Pressure Fields in an Enclosure with Two Openings in Natural Convection

Koueni, Toko Christian Anicet
Department of Renewable Energy, ENSPM,
University of Maroua, P. O. Box 46 Maroua, Cameroon

ABSTRACT

This work numerically studies the temperature and pressure fields generated by a solid heat source in an enclosure with an aspect ratio H/L = 0.82 having two symmetrical low openings in natural convection. The enclosure has a height H = 520 mm, a length L = 630 mm and a width l = 210 mm. The heat source is cylindrical with a diameter D0 = 20 mm and a length l = 210 mm. 04 values of the power per unit length were imposed on the heat source corresponding to 04 reduced Rayleigh numbers 0.59 × 1011, 1.78 × 1011, 2.19 × 1011 and 2.57 × 1011. 03 CAS 21, CAS 22, CAS 23 enclosures different by the position of the heat source were studied. In CAS 21, the heat source is at position x+ = 0.24, in CAS 22 at x+ = - 0.24 and in CAS 23 at position x+ = 0. The study was carried out in steady state. Numerical studies were conducted by DNS considering that the heat source is at constant power per unit length. Numerical results show that in CAS 23 and whatever the values of the reduced Rayleigh number, the thermal plume is centered at a higher temperature than that of the environment outside the plume. The thermal plume is generated by turbulent natural convection. Its initial speed is a function of the speed of fresh air entering the enclosure through the openings and its initial temperature is a function of the reduced Rayleigh number. The gas movements at the openings are created by the static pressure difference between the inside and outside of the enclosure. In the CAS 21 enclosure, the thermal plume is deflected from x+ > 0 and in CAS 22 from x+ < 0. This deflection of the thermal plume towards one of the side walls of the enclosure may be due to the Coanda effect. The numerical results of the temperature and the differential static pressure agree with the experimental measurements.

Keywords: Enclosure with aspect ratio less than 1, Natural convection, Solid heat source, Temperature fields, Pressure fields, Numerical calculation.

INTRODUCTION

Natural convection is a phenomenon of fluid mechanics, which occurs when a gradient induces a movement in the fluid. The gradient can concern different intensive quantities such as temperature ("thermal convection"). Since the density depends on the temperature, a temperature gradient generates differences in density within the fluid, resulting in lateral variations in the Archimedes' thrust which are at the origin of the movement. Such displacements are called convection movements. These natural convection movements are present in many industrial processes such as: pipes, electrical cabinets where they participate in the cooling of electronic components, Le Masson et al. (2011) [1], transformers, sensors and solar and electric dryers. They are also found in the building sector (offices, classrooms,

supermarkets, conference rooms, etc.). Their action is fundamental in heating, air conditioning of premises, drying of wood, clothes... And it also helps to explain the flows that develop in compartment fire situations, Karlsson and Quintiere (2000) [2], Quintiere et al. (1981) [3].

In this study, we will focus on natural convection in enclosures with openings with an internal heat source. In these enclosures, initially the enclosure is in equilibrium with the external environment. As soon as the heat source is turned on, the heat source heats the enclosure by natural convection and creates a static pressure difference between the inside and the outside of the enclosure which generates gas exchanges at the openings [4 – 9]. The heat source can have several positions in the enclosure and can be located either near the floor of the enclosure [4 – 9], or on one of the vertical walls [10, 11]. Or outside the enclosure (infinite reservoir of hot air) [12]. Miyamoto et al. (1989) [13], Prakash et al. (2012) [14] examined the influence of the aspect ratio of the openings on heat transfer. The enclosure can have several symmetrical or asymmetrical openings, have an aspect ratio less than or greater than 1. For aspect ratios greater than 1, the dynamic fields [3], the temperature fields [4, 5], [8, 9] and the pressure fields have been studied [7]. The studies being either numerical [4 – 9], or experimental [4], or analytical [4]. When the aspect ratio is less than 1, KOUENI TOKO (2019) [4] experimentally showed that the filling of gases in the enclosure presents a similarity with that of the "filling box" of Baines and Turner (1969) [15] only in the initial heating phase. As soon as the interior of the enclosure is heated, the changes in static pressure induce gas exchanges with the outside which result in heating of the region located around the plume.

In this work, we will study numerically the temperature and pressure fields in 03 CAS 21, CAS 22 and CAS 23 enclosures with 02 openings in natural convection. These 03 enclosures with aspect ratio $H/L = 0.82$ differ from the position of the heat source on the floor. In CAS 21, the heat source is at $x+ = 0.24$, in CAS 22 at $x+ = -0.24$ and in CAS 23 at the position $x+ = 0$. 04 powers per unit length have been imposed on the heat source corresponding to 04 reduced Rayleigh number 0.59×10^{11}, 1.78×10^{11}, 2.19×10^{11} and 2.57×10^{11}. This study has never been carried out and will be done in steady state.

EXPERIMENTAL DEVICE

03 CAS 21, CAS 22 and CAS 23 enclosures constitute the experimental devices studied in this work. These enclosures differ in the position of the heat source near the floor of the enclosure. In CAS 21 the heat source is at position $x+ = 0.24$, in CAS 22 at $x+ = -0.22$ and in CAS 23 at position $x+ = 0$ (Figure 1). These enclosures are composed of 02 openings symmetrical with respect to the axis (0x+) and located at the bottom of the enclosure near the floor on the two side walls parallel to the heat source. These openings have the same height $h = 34\ mm$ and the same width $l = 210\ mm$. These enclosures are parallelepiped with height $H = 520\ mm$, length $L = 630\ mm$ and width $l = 210\ mm$. The aspect ratio of these enclosures is $H/L = 0.82$. The heat sources of these enclosures are solid, cylindrical with diameter $D_0 = 20\ mm$, length $l = 210$ mm. These heat sources have the same time constant different from 0 and are made of stainless steel. A Neumann condition of constant power per unit length is imposed on the heat sources. 04 powers per unit length were imposed corresponding to 04 reduced Rayleigh numbers (Table 1). These enclosures were used for the numerical calculations of our work.

Table 1: Rayleigh number reduced as a function of the power of the heat source

Φ (W/m)	*Ra**
100	0.59×10^{11}
180	1.16×10^{11}
275	1.78×10^{11}
340	2.19×10^{11}
400	2.57×10^{11}

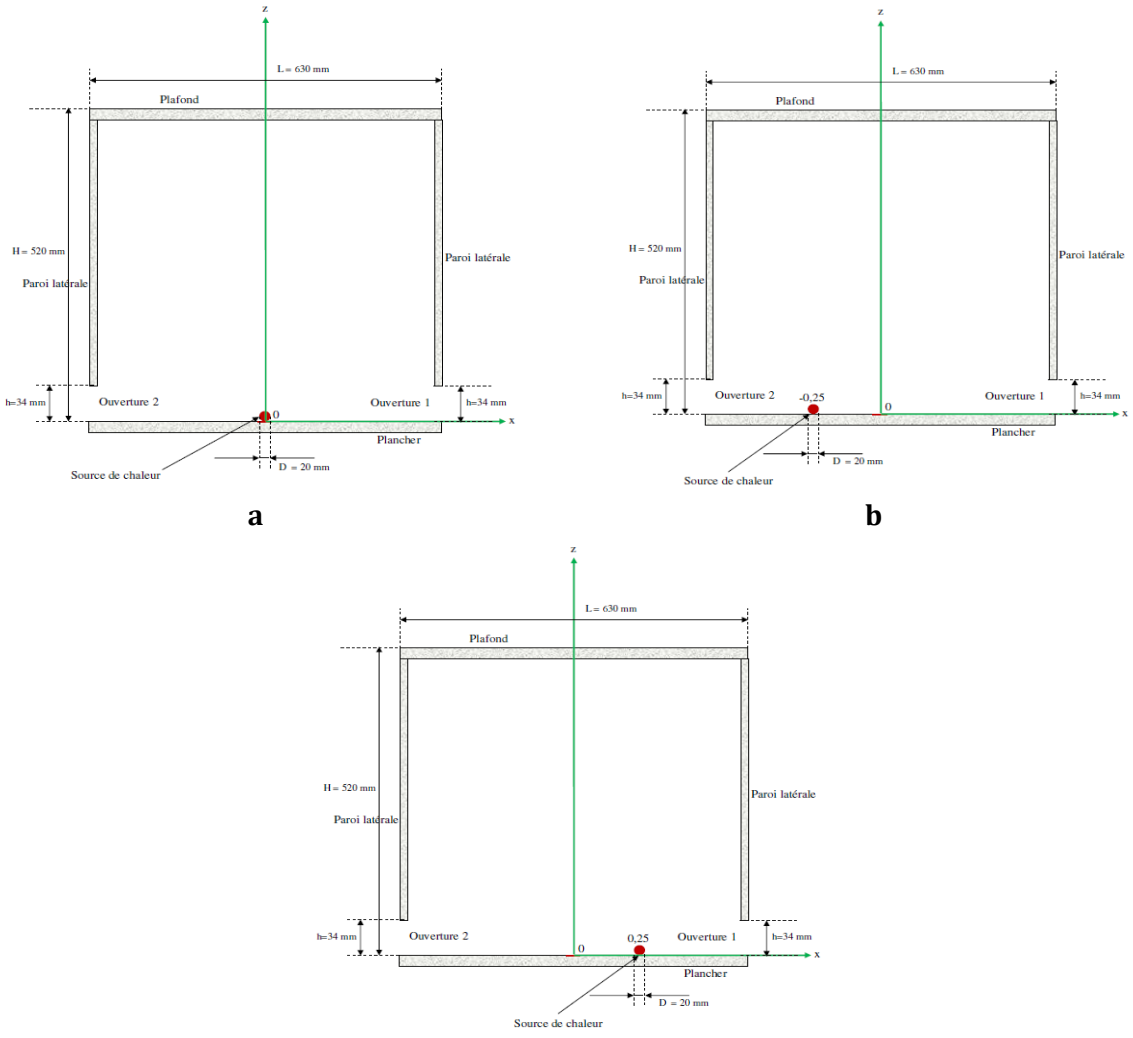

Figure 1: Experimental devices a) CAS 23, b) CAS 22, c) CAS 21

These enclosures have a 03-dimensional orthonormal Cartesian axis system with center 0. The (0x+) axis is the abscissa axis, the (0y+) axis is the ordinate axis and the (0z+) axis is perpendicular to the plane formed by the (0x+) and (0y+) axes. The heat source is 3 mm above the floor of the enclosures which are made of plexiglass of the same materials as all the other walls of the enclosures. The floors have a thickness of 14 mm, identical to that of the ceilings of the enclosures. The side walls are each 8 mm thick. The walls of the enclosures are assembled

with glue. Initially, the enclosures are in equilibrium with the external environment. As soon as the heating system is started, the enclosures are heated by natural convection which creates a static pressure difference between the inside and the outside of the enclosures [4]. The thermal plume is turbulent.

The expression for the reduced Rayleigh number is:

$$Ra^* = \delta^2 Ra \quad (1)$$

With

$Ra = Gr \times Pr = \frac{C_P \times g \times \beta \times H^3 \times \varphi_0 \times \rho}{\upsilon \times {\lambda_g}^2}$: Rayleigh number;

$\varphi_0 = h \times (T_0 - T_{ext})$: Heat flow per unit length;

$h\ \left(\frac{W}{mK}\right) = \lambda_g$: Convection heat coefficient near the heat source;

$\delta = \frac{\mathrm{L}}{\mathrm{H}} = 1{,}21$: Inverse of aspect ratio;

$Gr = \frac{g \times \beta \times H^3 \times \varphi_0}{\lambda_g \times \nu^2}$: Grashof number;

$Pr = \frac{\nu}{\alpha}$: Prandtl number;

EXPERIMENTAL MEASUREMENTS OF TEMPERATURE AND PRESSURE

Experimental Temperature Measurements

To record the temperature measurements taken inside the CAS 23 enclosure, we used a "National Instrument" acquisition card that converts the analog signal (voltage) coming from the thermocouples into a numerical signal (voltage) controlled by a computer. Using Labview software, the numerical signal (voltage) is converted into temperature and recorded on a USB key or a hard drive in an Excel file. This card consists of three (03) modules with 16 inputs each.

To simultaneously measure the temperature values over the entire height of the CAS 23 enclosure, we used a comb of forty-seven (47) thermocouples located:

- On verticals passing through the coordinate points: *x*=- 0.485; -0.2; 0.2* and *0.485; y* = 0* at heights *z* = 0.01; 0.06; 0.13; 0.25; 0.42; 0.66; 0.96*.
- On the vertical passing through the coordinate point: *x* = 0; y* = 0* at heights *z*= 0.13; 0.25; 0.42; 0.66; 0.96*.
- At the level of the side walls parallel to the heat source and the ceiling of the enclosure. At the openings, we have carried out occasional temperature measurements over time.

Experimental Measurements of Differential Pressure

Differential pressure measurements were performed in unsteady conditions or after steady state were established in the enclosure. These measurements were also performed before heating the enclosure to test the accuracy of these measurements. In the latter case, ΔPmes (z) is always close to zero. In order to be able to successively measure the differential pressure at different heights with a single micromanometer, we used a Furness Control scanner of the FCS 421 type. This selection box allows connecting up to twenty different wall pressure readings to

the same micromanometer. However, since only one micromanometer is available, this procedure requires about fifteen minutes to carry out ten measurement points. The differential pressure measurement was carried out on the CAS 23 model at the positions *x* = - 0.485; 0 and 0.485*.

For these pressure difference measurements, one of the vertical walls is pierced with a series of 20 pressure taps distributed over three verticals located at positions *x* = - 0.485; 0 and 0.485*. On the verticals located at positions *x* = - 0.485 and 0.485,* we have seven pressure taps 90 mm apart outside the openings and 20 mm apart at the openings. On the vertical located at position *x* = 0*, we have six pressure taps 90 mm apart. These pressure taps are made using small diameter orifices (0.5 – 1 mm) drilled in the wall.

MATHEMATICAL MODEL AND NUMERICAL METHOD

Mathematical Model

The characteristic equations of the phenomenon studied take into account the confinement of the enclosure characterized by the inverse of the aspect ratio δ. These equations were developed by KOUENI *et al.* [5] and grouped into the mass conservation equation ((5), the momentum conservation equation (6) and the energy conservation equation (7). These equations consider that the fluid is viscous compressible and the density of the fluid takes into account the Boussinesq hypothesis. The thermal conductivity and dynamic viscosity of the fluid depend on the temperature of the fluid. These equations were established in a steady state and dimensionless. The equations were established by considering that the heat source is solid with a non-zero time constant and that we are in natural convection. It is the generation of the turbulent thermal plume by the movements of gases at the openings and the power of the heat source which is at the origin of the phenomena present in the studied enclosures. The reduced Rayleigh numbers (1) and reduced Grashof numbers (9) represent the buoyancy flux created by the heat source when it is subjected to a constant power per unit length. The Boussinesq approximation was considered in the thermal plume characterized by density (3). Outside the thermal plume the density varies with temperature (2). The materials of the heat source, side walls, floor and ceiling as well as their thicknesses were considered. Conduction at the walls was considered.

Heat transfer by radiation being neglected.

$$\rho = \rho(T) \tag{2}$$

Expression (3) of buoyancy is defined by Morton *et al.* [16].

$$\frac{\rho_0 - \rho}{\rho_1} = \beta(T - T_0) \tag{3}$$

With
ρ_1: Reference density;
ρ_0: Outside density of enclosure;
T_0: Outside temperature of enclosure.

For a gas, β is given by the expression (4)

$$\beta \sim \frac{1}{T_1} \tag{4}$$

T_1: Reference temperature.

According to KOUENI *et al.* [5], the expression of the Boussinesq approximation is $|\delta\rho| \ll \rho_0$ ($\frac{\rho_0}{\rho} \approx 1$). The dimensionless conservation equations of mass (5), momentum (6) and energy (7) [4, 5] are:

$$\rho\left(\frac{1}{\delta}\frac{\partial u^+}{\partial x^+} + \frac{1}{\delta}\frac{\partial v^+}{\partial y^+} + \frac{\partial w^+}{\partial z^+}\right) = 0 \tag{5}$$

$$\begin{cases} \frac{u^+}{\delta}\frac{\partial u^+}{\partial x^+} + \frac{v^+}{\delta}\frac{\partial u^+}{\partial y^+} + w^+\frac{\partial u^+}{\partial z^+} = -\frac{1}{\delta}\frac{\partial P^+}{\partial x^+} + \frac{1}{Gr^{*1/2}}\left(\frac{\partial^2 u^+}{\partial x^{+2}} + \frac{\partial^2 u^+}{\partial y^{+2}} + \delta\frac{\partial^2 u^+}{\partial z^{+2}}\right) \\ \frac{u^+}{\delta}\frac{\partial v^+}{\partial x^+} + \frac{v^+}{\delta}\frac{\partial v^+}{\partial y^+} + w^+\frac{\partial v^+}{\partial z^+} = -\frac{1}{\delta}\frac{\partial P^+}{\partial y^+} + \frac{1}{Gr^{*1/2}}\left(\frac{\partial^2 v^+}{\partial x^{+2}} + \frac{\partial^2 v^+}{\partial y^{+2}} + \delta\frac{\partial^2 v^+}{\partial z^{+2}}\right) \\ \frac{u^+}{\delta}\frac{\partial w^+}{\partial x^+} + \frac{v^+}{\delta}\frac{\partial w^+}{\partial y^+} + w^+\frac{\partial w^+}{\partial z^+} = -\frac{1}{\delta}\frac{\partial P^+}{\partial z^+} + \frac{1}{Gr^{*1/2}}\left(\frac{\partial^2 w^+}{\partial x^{+2}} + \frac{\partial^2 w^+}{\partial y^{+2}} + \delta\frac{\partial^2 w^+}{\partial z^{+2}}\right) - T^+ \end{cases} \tag{6}$$

$$\frac{u^+}{\delta}\frac{\partial T^+}{\partial x^+} + \frac{v^+}{\delta}\frac{\partial T^+}{\partial y^+} + w^+\frac{\partial T^+}{\partial z^+} = \frac{1}{(PrRa^*)^{1/2}}\left(\frac{\partial^2 T^+}{\partial x^{+2}} + \frac{\partial^2 T^+}{\partial y^{+2}} + \delta\frac{\partial^2 T^+}{\partial z^{+2}}\right) \tag{7}$$

Where

$$x^+ = \frac{x}{L}, y^+ = \frac{y}{L}, z^+ = \frac{z}{H}, u^+ = \frac{u}{U_0}, v^+ = \frac{v}{U_0},$$

$$w^+ = \frac{w}{U_0}, T^+ = \frac{T - T_{ext}}{T_0 - T_{ext}}, \text{ et } P^+ = \frac{P}{|P_{max}|}$$

With

$$U_0 = \sqrt{\frac{P_{max}}{\rho_\infty}} \tag{8}$$

According to KOUENI et al. [5], the equation (8) is the maximum velocity air inlet cool into the enclosure.

The reduced Grashof number is:

$$Gr^* = \delta^2 Gr \tag{9}$$

Numerical Method

Direct numerical simulation (DNS) was used to solve the equations of the physical problem of our study. It uses the finite volume method [9]. The mathematical equations used to solve our

physical problem are discretized and form a system of algebraic equations [17]. The discretization scheme used to solve the momentum and energy conservation equations is the QUICK scheme [18]. To solve the pressure, we considered the "Weighted Body Force" scheme [5] [8] [9] [19]. Spalding and Patankar established the SIMPLE algorithm. This algorithm corrects the pressure on a non-uniform mesh. We used the SIMPLE algorithm to solve the pressure-velocity coupling problem [9]. The temperature and pressure solutions were obtained by the commercially available FLUENT computational code. This code is based on the execution of a Gauss Seidel linear system algorithm based on the AMD multi-grid algebraic method. The resolution of the steady-state equations is done by iteration considering the conduction in the side walls, the floor and the ceiling.

According to KOUENI TOKO (2022) [6], The final solution of the problem is obtained by doing a test on the convergence by comparing the value obtained at the current iteration to the value of the previous iteration of the kind:

$$\frac{w_i - w_{i-1}}{w_{i-1}} \leq \epsilon \quad (10)$$

With

- i: Number of iterations.

A convergence test was applied to the variables u, v and w. ε is the relative error, it characterizes the degree of precision of the final solution. If the test is negative, we do a second update w_{i-1} takes w_i and the calculation operations start again in the initial state. If the test is positive, the results are saved and the calculation stops. For our calculations, we have given ε the value 10^{-5}.

The mesh considered is regular, fine non-uniform with a number of meshes of 1683171. This mesh allows having a stable solution close to reality. The meshes of the CAS 21, CAS 22, CAS 23 enclosures are shown in Figure 2. The calculation stops after the convergence of the continuity, temperature and velocity equations (u, v and w). To have a stable solution and reduce the calculation times of the temperature, velocity and pressure, we studied the impact of the number of meshes (Table 2) on the solution in temperature and pressure (Figure 4). According to Figure 4, the optimal mesh is the normal mesh (Table 2).

Table 2: Characteristics of Numerical devise meshes

Meshes	Coarse mesh	Normal mesh	Fine mesh
Cells	931393	1683171	3279665
Nodes	331884	583553	1142316

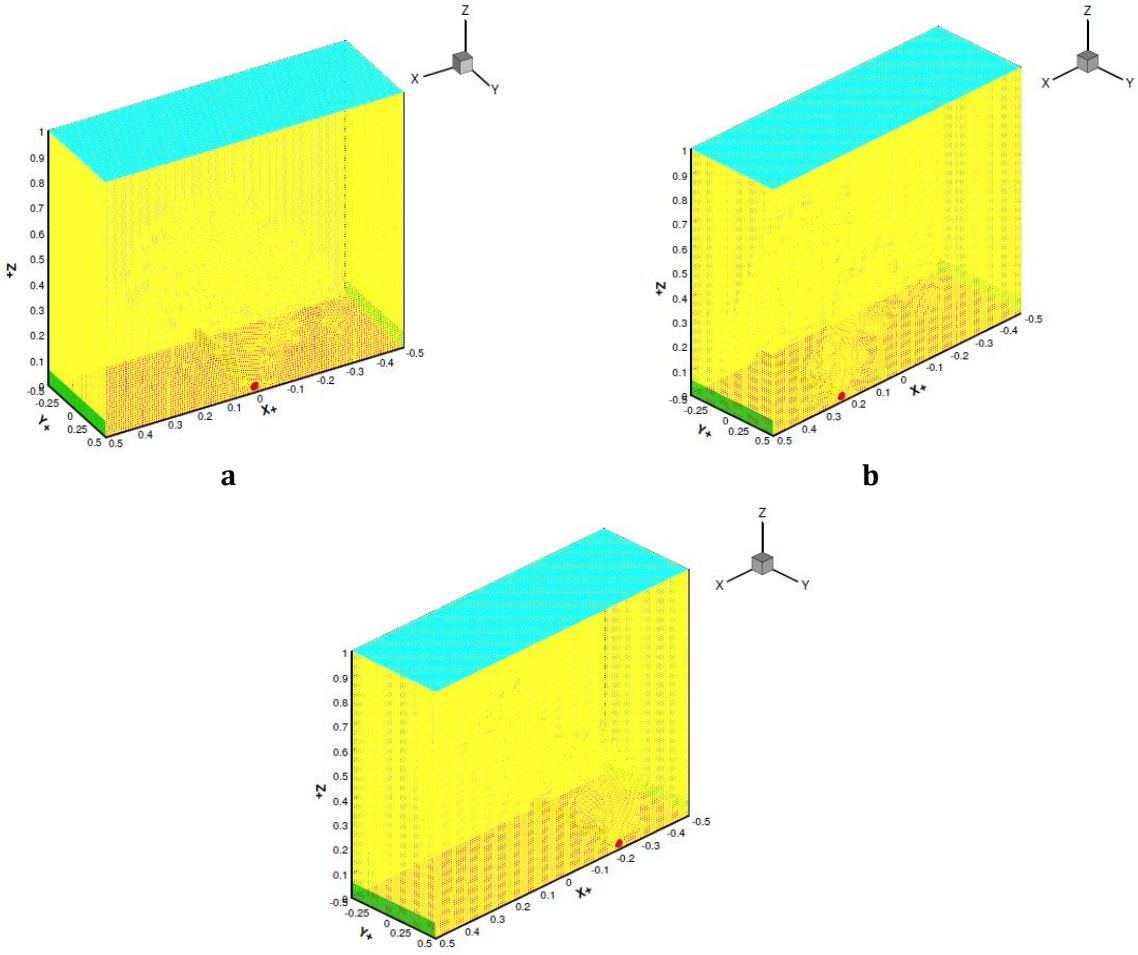

a b

c

Figure 2: Meshing of the numerical calculations devices. a) CAS 23, b) CAS 22 c) CAS 21

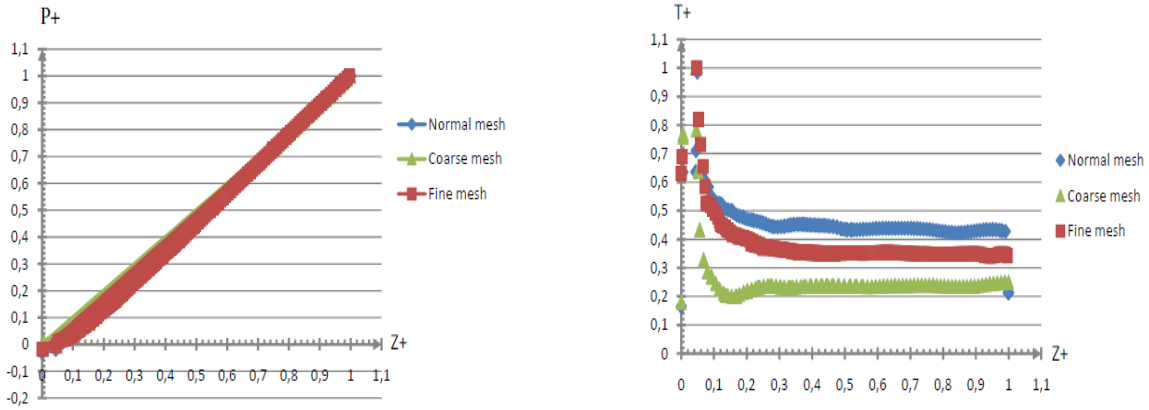

a b

Figure 4: Impact of the number of meshes on the temperature profiles T+ and differential static pressure P+ obtained in the CAS 23 configuration at position x+ = 0, y+= 0, Ra* = 1.78×1011, a) Pressure profiles, b) temperature profiles

To carry out our numerical calculations we used a laptop with maximum operating speed of CPU - 2 GHz, an Intel® Core ™ i3-5005U Processor, Ram - 4GB, x64 processor, Graphics card - Intel HD Graphics 5500 (300 - 850MHz), Number of transistors - 1300 million. The CPU time is 60 s.

Boundary Conditions

Initially, the temperature of the heat source is at constant flux per unit length and the static pressure difference between the inside and outside of the enclosure is zero at the enclosure openings. 04 reduced Rayleigh numbers were imposed: 0.59×10^{11}, 1.78×10^{11}, 2.19×10^{11} and 2.57×10^{11}. The boundary conditions on the studied enclosures CAS 21, CAS 22, CAS 23 are shown in Figure 3.

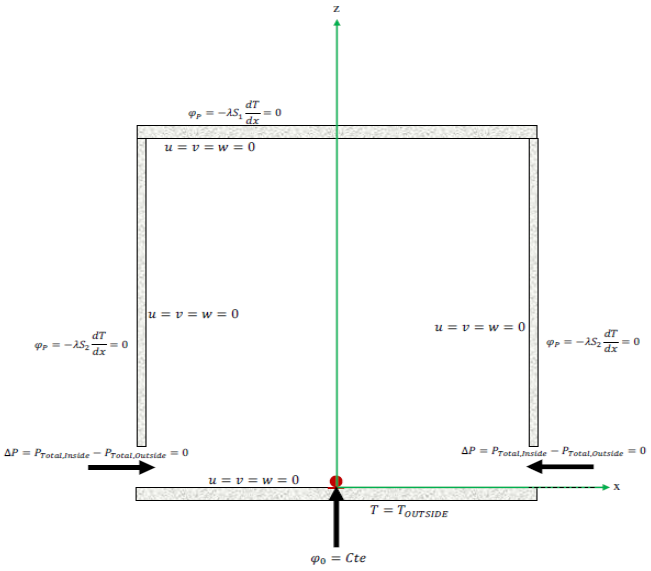

Figure 3: Boundary conditions

This Figure shows that a Newman condition is imposed on the side walls and the ceiling. A constant temperature condition is imposed on the floor. A constant flux per unit length condition is imposed on the heat source. A zero pressure difference condition is imposed on the openings.

On the heat source, the side walls, the floor and the ceiling, the axial, vertical and longitudinal velocities are zero. The expression of the total pressure at the openings of the enclosures is:

$$P_{total} = P_{stat} + \rho \frac{V^2}{2g} + \rho g z \quad (11)$$

RESULTS AND DISCUSSION

The results of the study of the temperature, pressure, velocity fields of the Nusselt number as a function of the reduced Rayleigh number Ra* and the position of the heat source position are presented in this part. The results of the comparison of experimental measurements and numerical calculations of the temperature and pressure fields are presented in this part.

Influence of the Reduced Rayleigh Number on Temperature Fields

Figure 5 shows the temperature fields obtained by numerical calculations for 04 reduced Rayleigh number Ra* = 0.59×1011, 1.78×10^{11}, 2.19×10^{11}, 2.57×10^{11}. This figure shows that when Ra*, the thermal plume remains centered in the CAS 23 configuration enclosure. The thermal plume reaches the ceiling of the enclosure where it is destroyed by shear, spreads over the ceiling and descends into the enclosure near the side walls. Close to the floor and outside the heat source, the temperature in the enclosure is close to the outside temperature. This may be due to the entry of fresh air into the enclosure through the openings. The temperature in the enclosure near the ceiling is higher than the outside temperature, because the thermal plume destroyed at the ceiling increases the temperature of the gases in its vicinity. Figure 5 shows three (03) temperature zones outside the thermal plume. In zone 1 near the floor, the temperature is almost constant and close to the outside temperature. In zone 2 between *z+ = 0.02 and 0.2* (Figures 5a, 5b and 5d) and between *z+ = 0.02 and 0.1* (Figure 5c), the temperature is stratified and higher than the temperature in zone 1. Zone 3 is between *z+ = 0.2 and 1* (Figures 5a, 5b and 5d) and between *z+ = 0.1 and 1* (Figure 5c), its temperature is almost constant and higher than the temperature in zone 2. The temperature in the thermal plume is higher than the temperature of the enclosure and outside the plume.

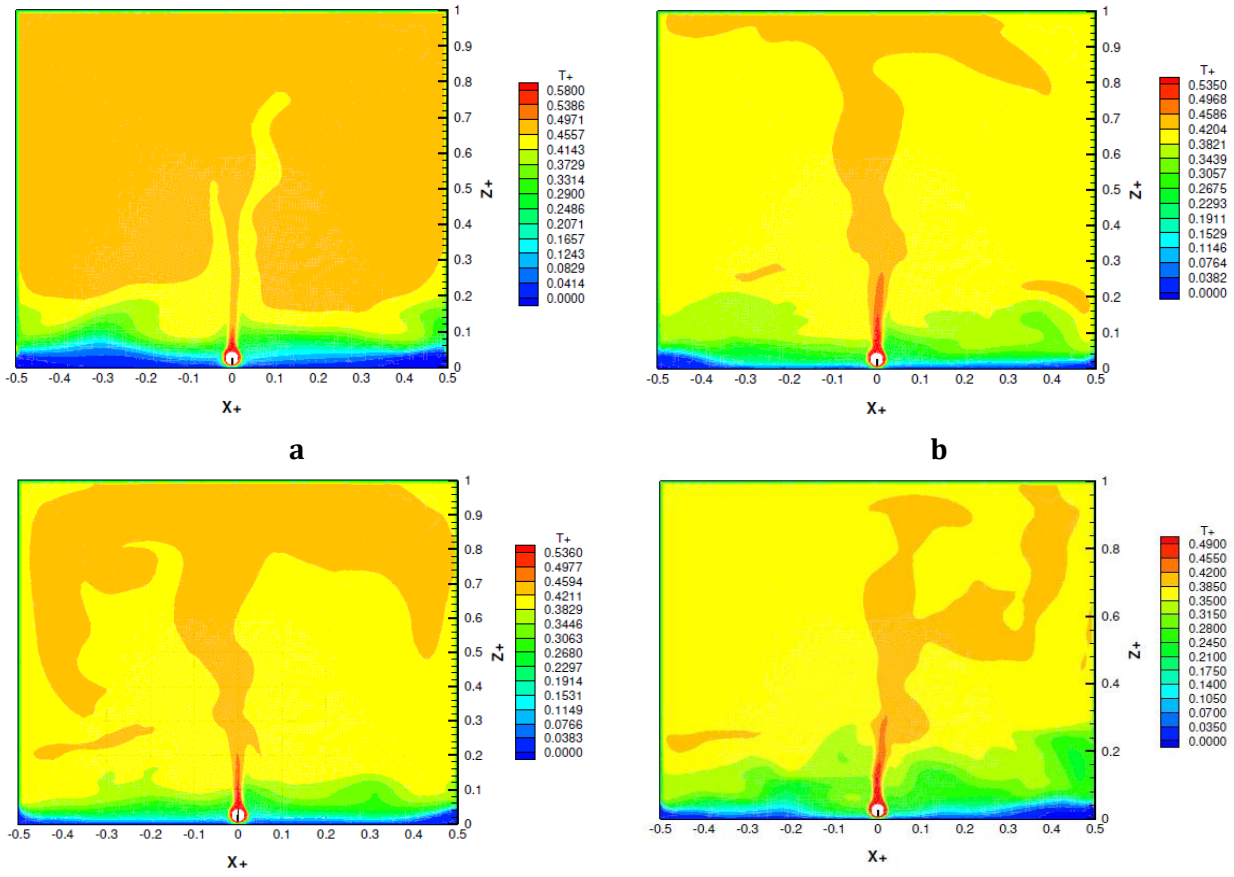

Figure 5: Temperature fields obtained in the CAS 23 configuration enclosure by numerical calculations and at the position y+= 0, a) Ra* = 0.59×10^{11}, b) Ra* = 1.78×10^{11}, c) Ra* = 2.19×10^{11}, d) Ra* = 2.57×10^{11}

Figure 6 shows the temperature fields obtained by numerical calculations at the openings at positions z+ = 0.01 and 0.06 when the reduced Rayleigh numbers are 0.59×10^{11}, 1.78×10^{11}, 2.19×10^{11}, 2.57×10^{11}. It is clear from this Figure and outside the vicinity of the heat source that at position *z+ = 0.01* near the floor the temperature is close to the outside temperature, the air is cool and at position *z+ = 0.06*, close to the top of the openings the temperature is higher than the temperature. At this level, the gases are hot.

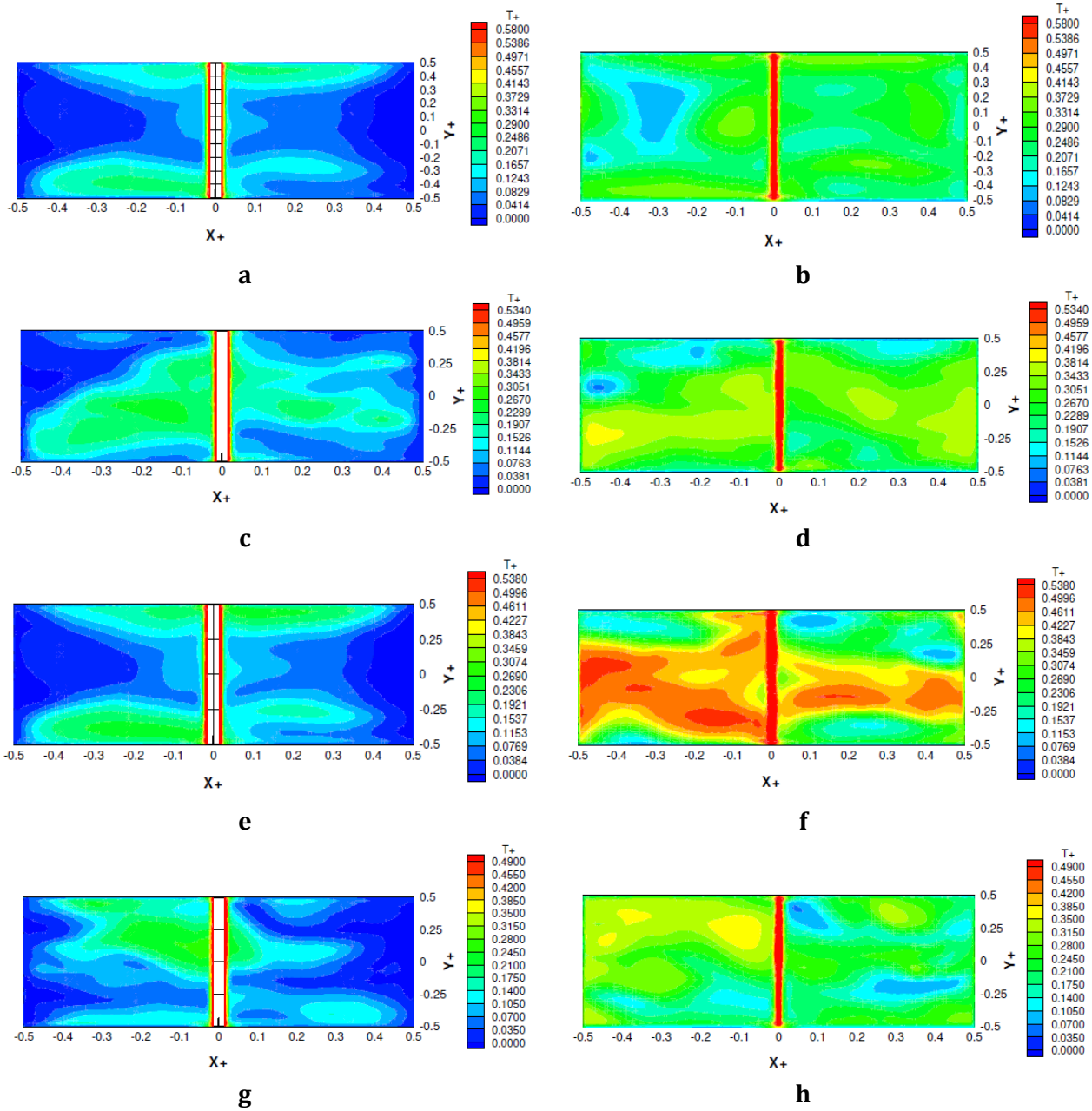

Figure 6: Temperature fields obtained by numerical calculations at the openings. a) z+ = 0.01, Ra* = 0.59×10^{11}, b) z+ = 0.06, Ra* = 0.59×10^{11}, c) z+ = 0.01, Ra* = 1.78×10^{11}, d) z+ = 0.06, Ra* = 1.78×10^{11}, e) z+ = 0.01, Ra* = 2.19×10^{11}, f) z+ = 0.06, Ra* = 2.19×10^{11}, g) z+ = 0.01, Ra* = 2.57×10^{11}, g) z+ = 0.06, Ra* = 2.57×10^{11}

Influence of the Reduced Rayleigh Number on Velocity Fields

Figure 7 shows the velocity fields along the direction of the (0x+) axis obtained at the openings of the CAS 23 enclosure by numerical calculations for 04 reduced Rayleigh numbers 0.59×10^{11}, 1.78×10^{11}, 2.19×10^{11}, 2.57×10^{11}. From this Figure we see that on the negative x+ side, at *z+ = 0.01* the velocity along the (0x+) axis is positive and at *z+ = 0.06*, it is negative. On the positive x+ side we observe the opposite phenomenon. From these observations, the air enters the enclosure through the bottom of the openings and the gases through the top of the openings. According to the reduced Rayleigh number studied we observe the same phenomenon.

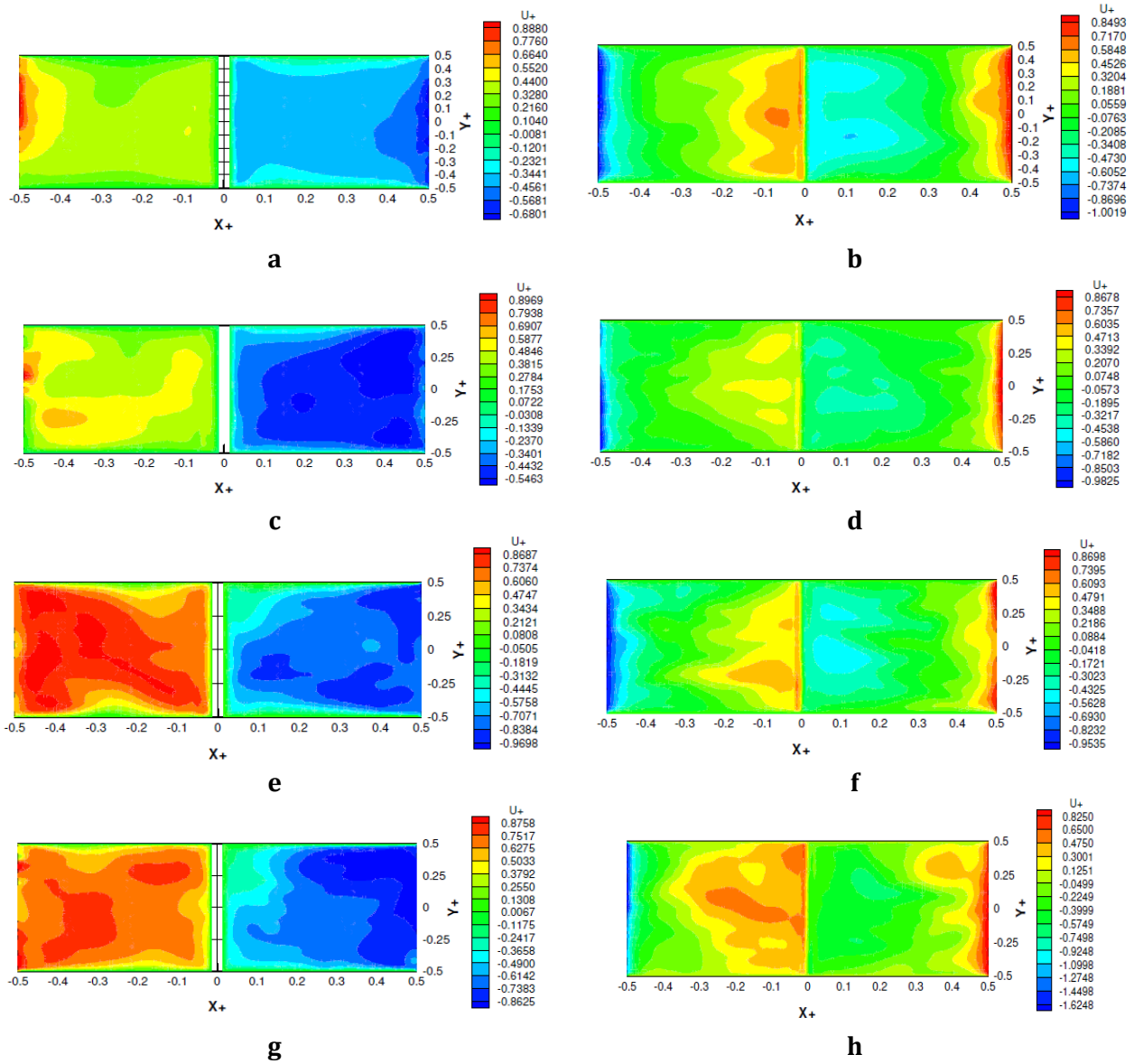

Figure 7: Velocity fields along the (0x+) axis obtained in the CAS 23 enclosure at the openings by numerical calculations. a) z+ = 0.01, Ra* = 0.59×10^{11}, b) z+ = 0.06, Ra* = 0.59×10^{11}, c) z+ = 0.01, Ra* = 1.78×10^{11}, d) z+ = 0.06, Ra* = 1.78×10^{11}, e) z+ = 0.01, Ra* = 2.19×10^{11}, f) z+ = 0.06, Ra* = 2.19×10^{11}, g) z+ = 0.01, Ra* = 2.57×10^{11}, g) z+ = 0.06, Ra* = 2.57×10^{11}

Influence of the Reduced Rayleigh Number on Temperature Profiles

Figure 9 shows the temperature profiles in the CAS 23 enclosure obtained by numerical calculations at position y+ when the reduced Rayleigh numbers are 0.59×10^{11}, 1.78×10^{11}, 2.19×10^{11}, and 2.57×10^{11}. This Figure shows that the temperature calculated at *x+ = 0* and at z+ between 0 and 0.2 is higher than the temperatures calculated at positions *x+ = - 0.49, - 0.36, - 0.24, 0, 0.24, 0.36, 0.49* and at z+ between 0 and 0.2 (Figures 9b, 9c, 9d). In Figure 9a we observe this phenomenon when z+ is between 0 and 0.1. For z+ between 0.1 and 1, this temperature difference approaches 0. When the reduced Rayleigh number increases from 0.59×10^{11} to 2.57×10^{11}, the same phenomenon is observed in the enclosure. At *z+ = 1*, the temperature values are lower than at *z+ = 0.95*, hence the existence of a thermal boundary layer close to the ceiling.

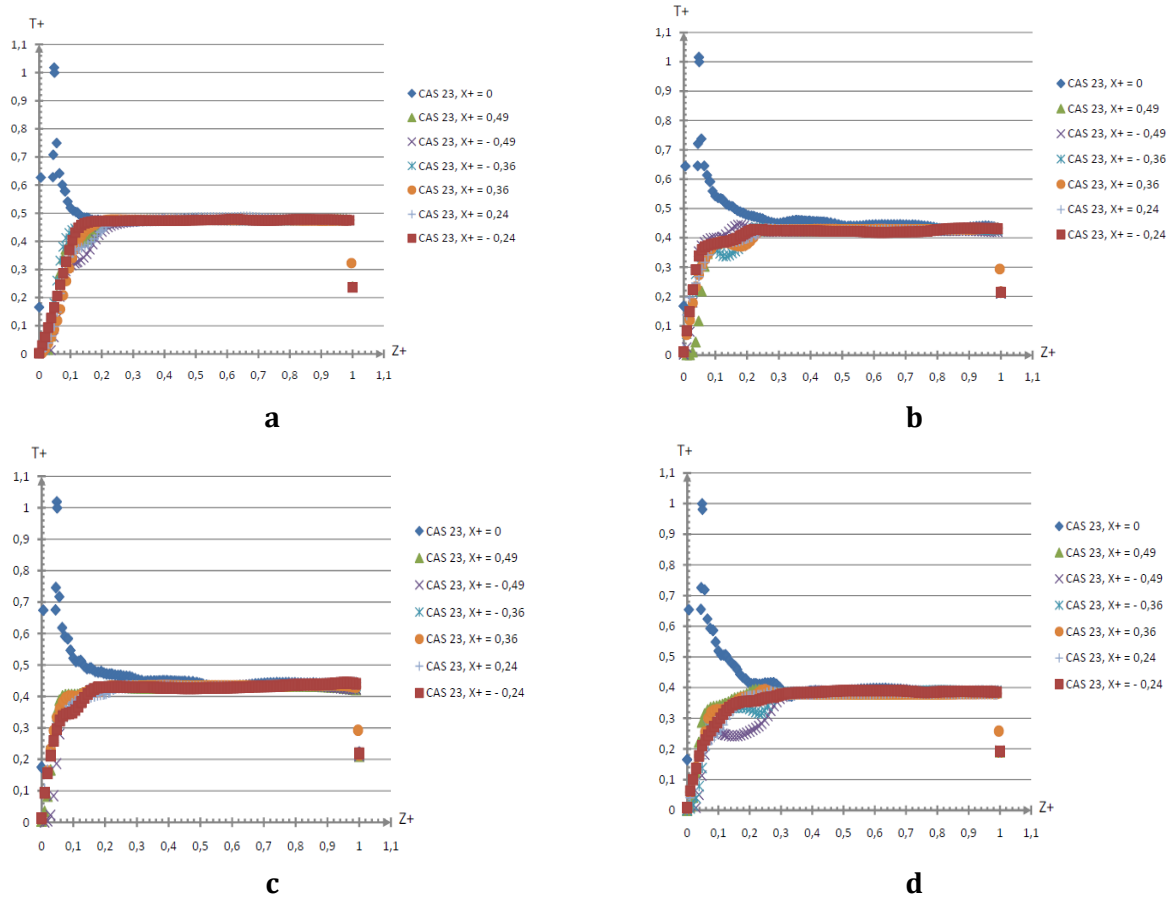

Figure 9: Temperature profiles obtained in the CAS 23 enclosure by numerical calculations at the position y+ = 0. a) Ra* = 0.59×10^{11}, b) Ra* = 1.78×10^{11}, c) Ra* = 2.19×10^{11}, d) Ra* = 2.57×10^{11}

Influence of the Reduced Rayleigh Number on Differential Static Pressures Profiles

Figure 8 shows the differential static pressure profiles obtained in the CAS 23 enclosure by numerical calculations at the position *y+ = 0*, when the reduced Rayleigh numbers are 0.59×10^{11}, 1.78×10^{11}, 2.19×10^{11}, 2.57×10^{11}.

It can be seen from this Figure that the differential static pressure values are low at the bottom of the enclosure and negative near the floor. These pressure values are high and positive near the ceiling of the enclosure. The negative differential static pressure values near the floor of the enclosure show that air enters the enclosure near the floor and gases exit the enclosure through the top of the openings because the differential static pressure values are positive. According to the increase in the reduced Rayleigh number, the same phenomenon is observed in the enclosure.

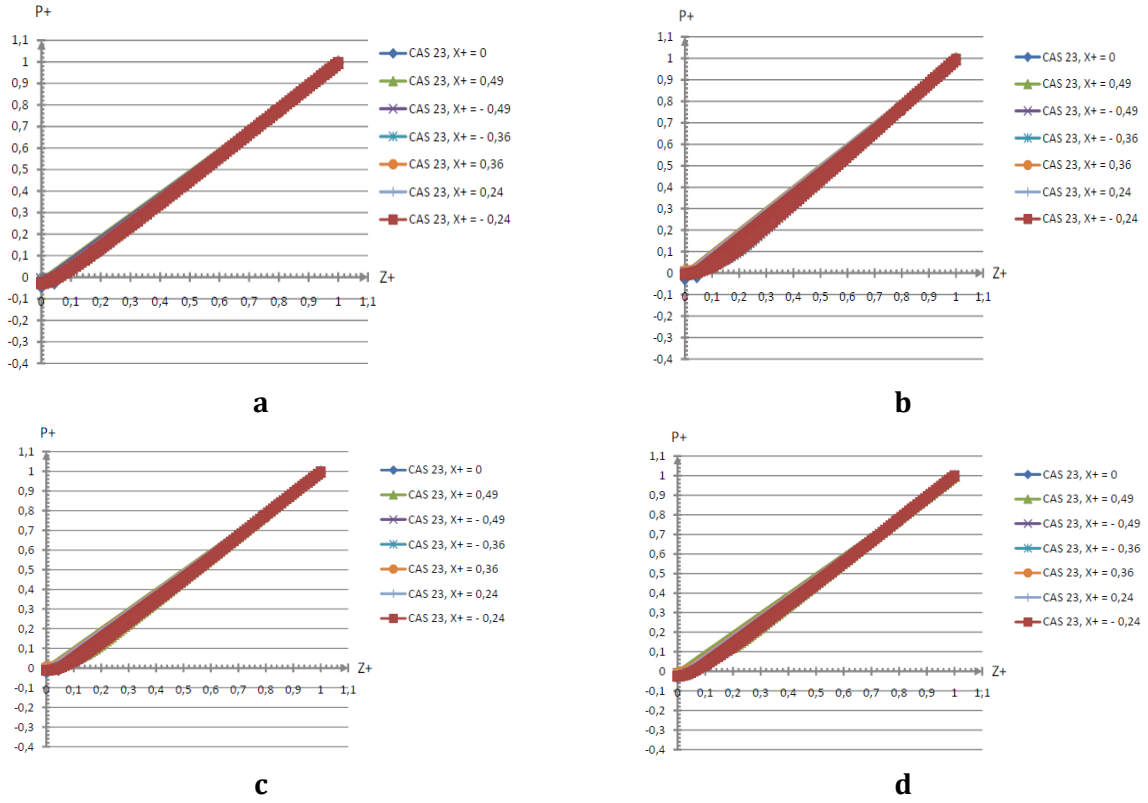

Figure 8: Differential static pressure profiles obtained in CAS 23 configuration by numerical calculations at position y+ = 0. a) Ra* = 0.59×10¹¹, b) Ra* = 1.78×10¹¹, c) Ra* = 2.19×10¹¹, d) Ra* = 2.57×10¹¹

Influence of the Position of the Heat Source on the Temperature Fields

Figure 10 shows the temperature fields obtained in the CAS 21, CAS 22 and CAS 23 enclosures by numerical calculations for 02 Rayleigh numbers 1.78×10¹¹, 2.19×10¹¹. From this Figure it appears that when the heat source is at position *x+ = 0*, the thermal plume in the enclosure is centered in the direction *0x+ = 0* (Figures 10a and 10b) and is not affected by the side walls. When the heat source is located at *x+ = 0.24*, the thermal plume is deflected to the side of *x+ > 0* (Figures 10c and 10d) near the right side wall. And is affected by this wall. When the heat source is at position *x+ = - 0.24*, the thermal plume is deflected to the side of *x+ < 0* (Figures 10e and 10f) towards the left side wall. And undergoes the effect of this wall. In the 03 enclosures studied, 03 thermal zones are observed outside the plume.

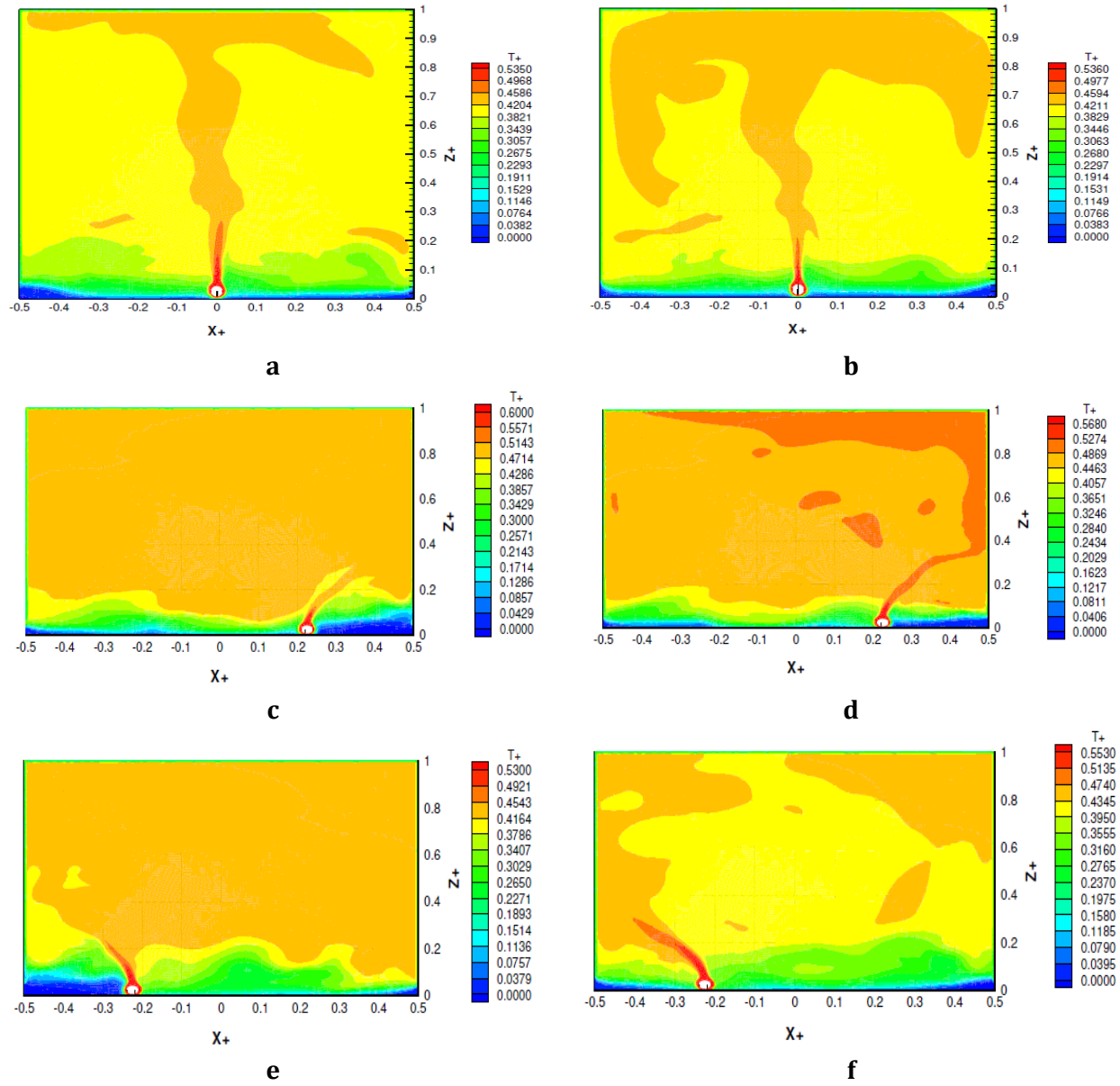

Figure 10: Temperature fields obtained by numerical calculations at the position y+ = 0 a) CAS 23, Ra* = 1.78×10¹¹, b) CAS 23, Ra* = 2.19×10¹¹, c) CAS 21, Ra* = 1.78×10¹¹, d) CAS 21, Ra* = 2.19×10¹¹, e) CAS 22, Ra* = 1.78×10¹¹, f) CAS 22, Ra* = 2.19×10¹¹

Zone 1 close to the cold floor at a temperature close to the outside temperature. A stratified zone 2 between *z+ = 0.02* and *z+ = 0.2* and a hot, quasi-homogeneous zone 3 between *z+ = 0.2 and 1*. On the side where the thermal plume is deflected, at the openings and when *Ra* = 1.78×10¹¹*, the temperature is close to the outside temperature (Figure 10c, 10e). When *Ra* = 2.19×10¹¹*, the same phenomenon is not observed.

Influence of Heat Source Position on Temperature and Differential Static Pressure Profiles

Figure 11 shows the differential static pressure profiles in the CAS 21, CAS 22, CAS 23 enclosures obtained by numerical calculations when the reduced Rayleigh number takes the values of 1.78×10^{11}, 2.19×10^{11}. It is noted that the static pressure profiles have the same shape and are grouped together.

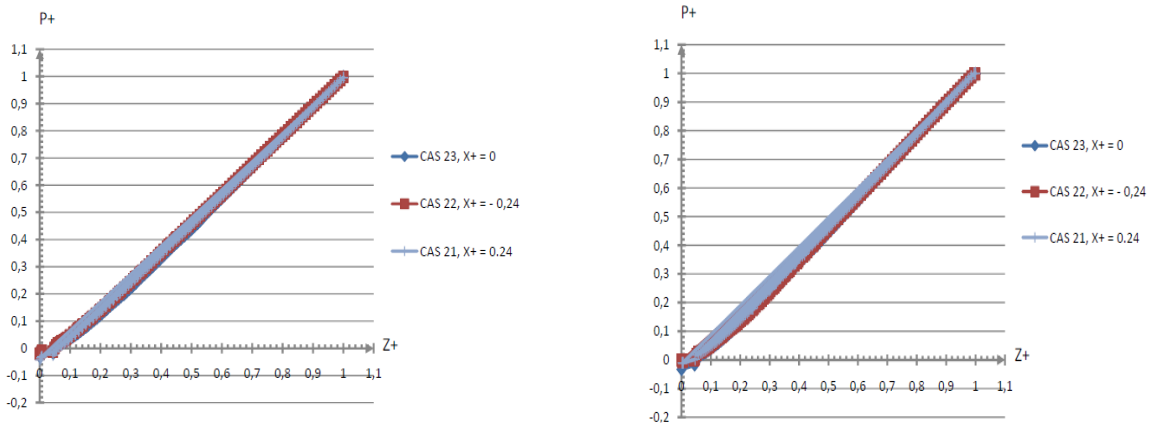

a **b**

Figure 11: Differential static pressure profiles obtained by numerical calculations at the position y+ = 0. a) Ra* = 1.78×10^{11}, b) Ra* = 2.19×10^{11}

Figure 12 shows the temperature profiles in the CAS 21, CAS 22, CAS 23 enclosures obtained by numerical calculations in the vertical line passing through the heat source at position *y+ = 0* and when the reduced Rayleigh number is 1.78×10^{11}, 2.19×10^{11}.

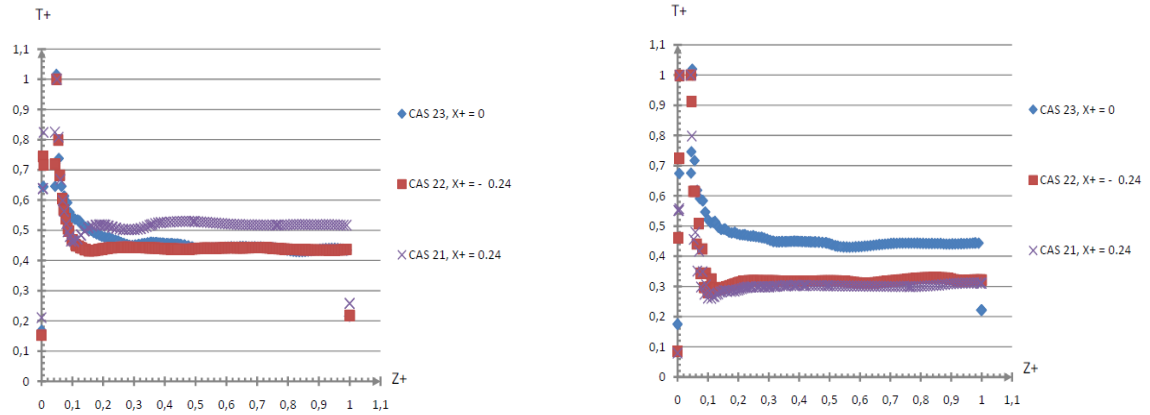

a **b**

Figure 12: Temperature profiles obtained by numerical calculations in the vertical passing through the heat source at the position y+ = 0. a) Ra* = 1.78×10^{11}, b) Ra* = 2.19×10^{11}

This Figure shows that the temperature profiles have the same shape and decrease from position *z+ = 0.01* to position *z+ = 1* regardless of the value of the reduced Rayleigh number. When *Ra* = 2.19×10^{11}, z+ > 0.1* the temperature values in the CAS 23 enclosure and at position *x+ = 0* are higher than those in the CAS 21 and CAS 22 enclosures in the vertical direction passing through the heat source.

Figure 13 shows the temperature profiles in the CAS 21, CAS 22 and CAS 23 enclosures obtained by numerical calculations outside the thermal plume at position *y+ = 0* and when the values of the reduced Rayleigh number are 1.78×10^{11}, 2.19×10^{11}.

It is noted that the temperature profiles have the same shape and increase from position *z+ = 0* to position *z+ = 1*.

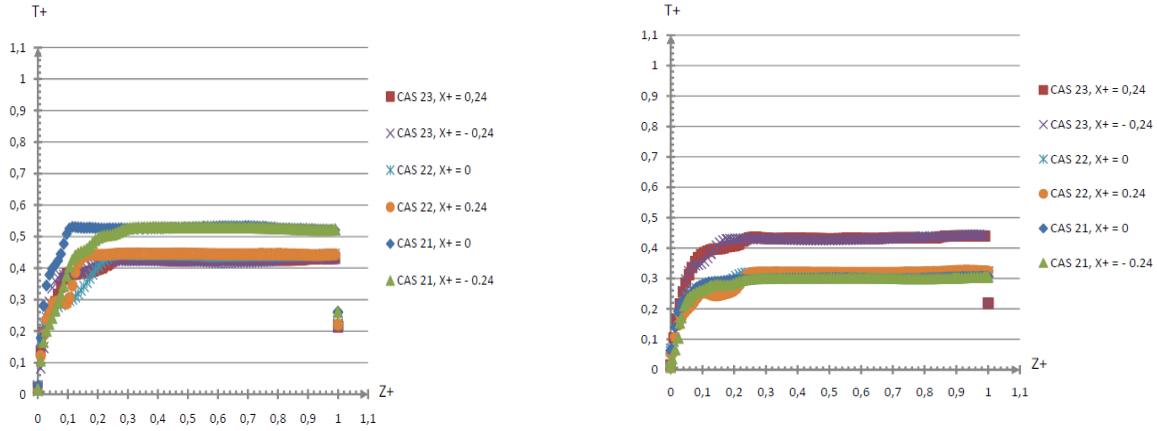

a **b**

Figure 13: Temperature profiles in CAS 21, CAS 22, CAS 23 enclosures obtained by numerical calculations outside the thermal plume at position y+ = 0. a) Ra* = 1.78×10^{11}, b) Ra* = 2.19×10^{11}

Influence of Reduced Rayleigh Number on Heat Source Temperature

Figure 14 shows the evolution of the temperature of the external surface of the heat source in the CAS 21, CAS 22, CAS 23 enclosures obtained by numerical calculations as a function of the reduced Rayleigh number.

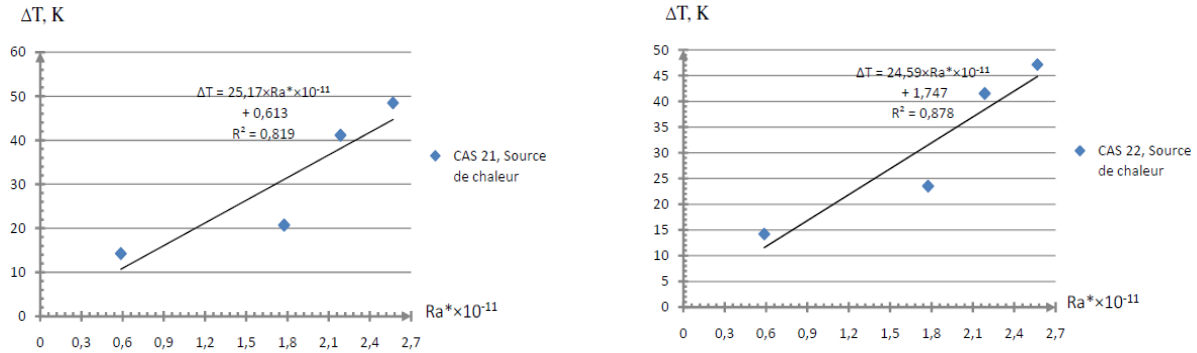

a **b**

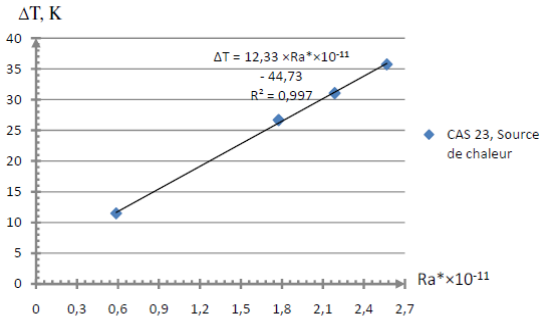

c

Figure 14: Evolution of the temperature of the heat source obtained by numerical calculations as a function of the reduced Rayleigh number. a) CAS 21, b) CAS 22, c) CAS 23

This Figure shows that the value of the temperature of the external surface of the heat source increases when the reduced Rayleigh number increases. This evolution, whatever the position of the heat source, is quasi-linear because the relative uncertainty is close to 1.

Influence of the Position of the Heat Source on the Nusselt Number

Figure 15 shows the evolution of the maximum Nusselt number in the vicinity of the heat source obtained by numerical calculations as a function of the reduced Rayleigh number.

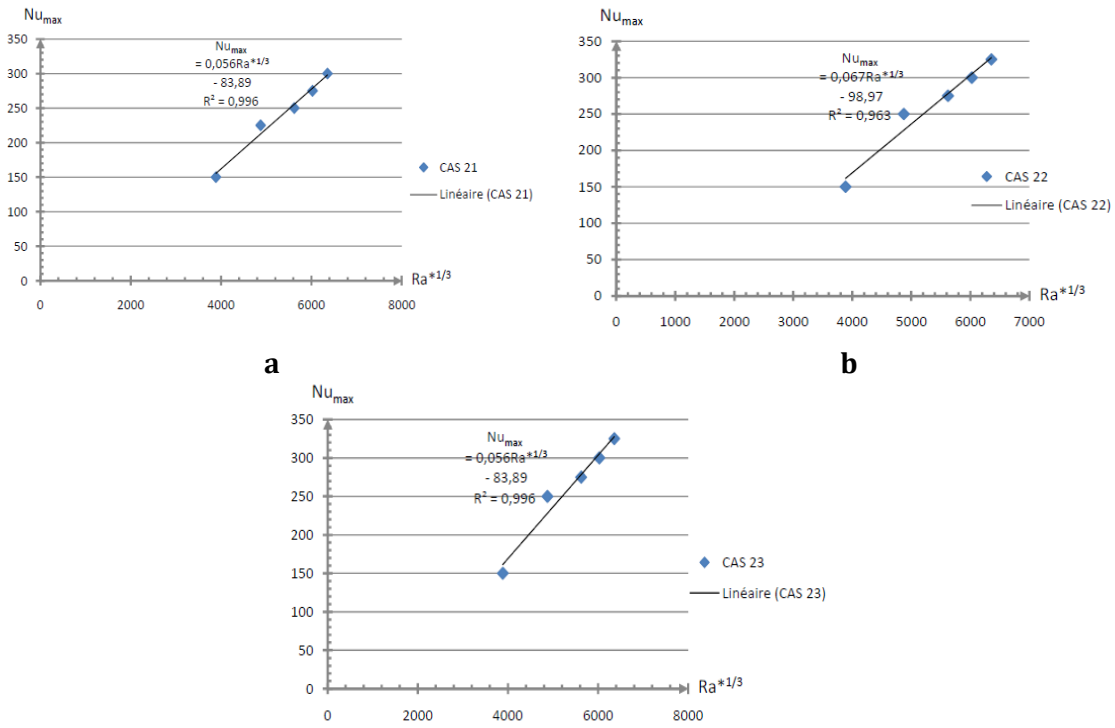

a **b**

c

Figure 15: Evolution of the maximum Nusselt number in the vicinity of the heat source obtained by numerical calculations as a function of the reduced Rayleigh number. a) CAS 21, b) CAS 22, c) CAS 23

This Figure shows that the Nusselt number increases when the reduced Rayleigh number increases. This evolution follows a linear law when the reduced Rayleigh number is at the power of 1/3, because the relative uncertainty tends towards 1 whatever the position of the heat source *x+ = - 0.24, 0, 0.24*.

Comparison of Differential Static Pressure and Temperature Obtained by Experimental Measurements with those from Numerical Calculations

Figure 16 compares the experimental temperature profiles in the CAS 23 enclosure with the numerical temperature profiles for 02 values of the reduced Rayleigh number $Ra^* = 1.78\times10^{11}$, 2.19×10^{11}. This Figure shows that the numerical temperature profiles have the same appearance as the experimental temperature profiles.

The experimental temperature measurements show that in the thermal plume the temperature values are higher than the temperature values outside the thermal plume. By numerical calculations, it is found that from *z+ = 0.2* the difference in temperature values in the thermal plume and outside is lower than experimentally. The experimental temperature measurements and the numerical calculations are in agreement.

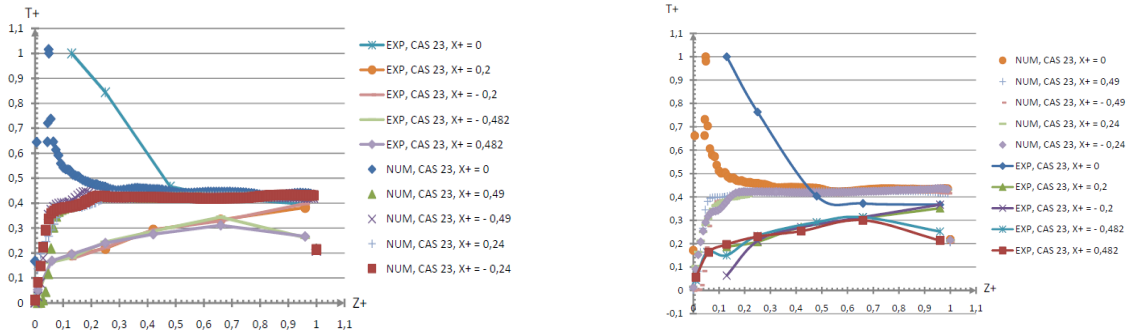

a **b**

Figure 16: Comparison of the temperature profiles in the CAS 23 enclosure obtained by numerical calculations with those of experimental measurements at the position y+ = 0. a) $Ra^* = 1.78\times10^{11}$, b) $Ra^* = 2.19\times10^{11}$

Figure 17 compares the experimental profiles of the differential static pressure in the CAS 23 enclosure with those of the numerical calculations for 02 reduced Rayleigh numbers $Ra^* = 1.78\times10^{11}$, 2.19×10^{11}. It can be seen that the experimental measurements of the differential static pressure agree with those of the numerical calculations.

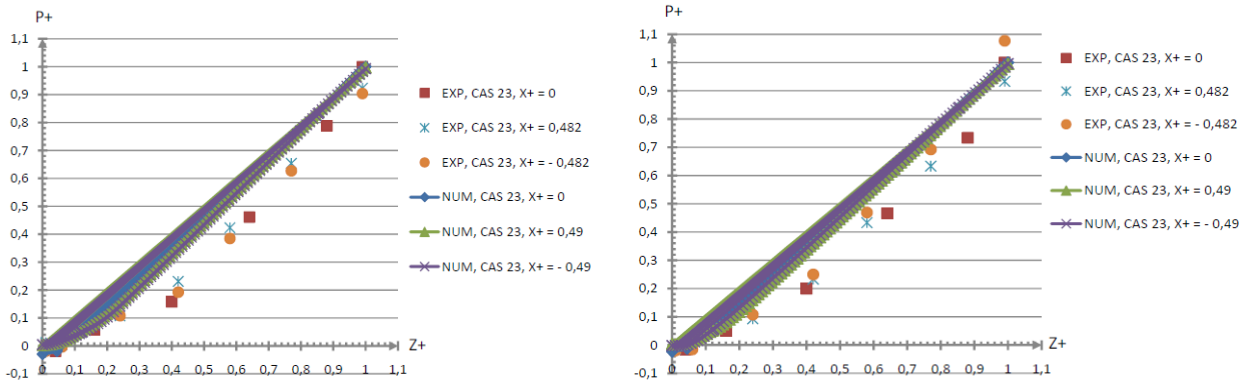

a **b**

Figure 17: Comparison of differential static pressure profiles obtained by numerical calculations with those of experimental measurements at the position y+ = 0. a) Ra* = 1.78×10¹¹, b) Ra* = 2.19×10¹¹

CONCLUSION

Ultimately, this work was about studying the temperature, pressure and velocity fields in 03 parallelepiped enclosures of length L, width l and height H, aspect ratio *H/L = 0.82* CAS 21, CAS 22, CAS 23 communicating with the environment outside the enclosure through 02 symmetrical openings with respect to the axis (0x+) and located on the floor. The enclosures are heated by linear heat sources with the same geometric characteristics. The 03 enclosures differ in the position of the heat source. In CAS 21 the heat source is at position *x+ = 0.24*, in CAS 22 at *x+ = -0.24* and in CAS 23 at *x+ = 0*. The heat source is solid, cylindrical with diameter $D_0 = 20$ *mm* and length *l = 210 mm*. 04 reduced Rayleigh numbers were considered $Ra^* = 0.59\times10^{11}$, 1.78×10^{11}, 2.19×10^{11}, 2.57×10^{11}. The generated thermal plume is turbulent. The Nusselt number is much higher than 1 therefore the heating is carried out in the CAS 23 enclosure by turbulent natural convection. Experimental temperature measurements were carried out in CAS 23 by a comb of 47 T-type thermocouples [4]. Differential pressure measurements were carried out in unsteady conditions or after steady state were established in the enclosure using pressure sensors [4]. Numerical studies were carried out by DNS for CAS 21, CAS 22, CAS 23 considering that the heat source is initially at constant heat flux per unit length and in steady state.

In CASE 23, the numerical results show that the thermal plume generated in the enclosure is centered, it does not undergo the effect of the side walls. Its starting point is the heat source and its arrival point is the ceiling of the enclosure. At the start, the thermal plume has a velocity w_0 and a temperature ΔT_0. The temperature ΔT_0 decreases from the surface of the heat source to the ceiling. The velocity w_0 of the gases forming the thermal plume is generated by the velocity u_0 of fresh air entering the enclosure through the openings. This fresh air entry is due to the negative static pressure difference between the inside and the outside of the enclosure close to the floor of the enclosure. At the ceiling of the enclosure the velocity $w_0 = 0$ *m/s*, the thermal plume is destroyed and the hot gases spread near the ceiling in the directions of $x+ > 0$ and $x+ < 0$. And descends towards the bottom of the enclosure where it exits the enclosure through the top of the openings at a velocity u_1. At the top of the openings, the static pressure difference between the inside and the outside of the enclosure is positive. The thermal plume

provides a heat flux ($\Phi_0 = \rho_0 S_0 w_0 C_P(\Delta T_0)$) to the environment outside the thermal plume which makes it possible to increase the temperature of this environment by receiving a heat flux Φ_1 ($\phi_1 = hS\Delta T_1$), heat transfers by conduction and radiation being neglected. Because assumed to be low compared to transfers by convection. Gases descending down the enclosure also exchange heat flux with the environment outside the thermal plume. The comparison of experimental measurements of temperature and differential static pressure agree with the numerical results in CAS 23.

When the heat source is at positions *x+ = - 0.24* (CAS 22), *x+ = 0.24* (CAS 21) the thermal plume is deflected towards one of the side walls (left CAS 22 and right CAS 21). This deflection of the thermal plume towards one of the side walls of the enclosure may be due to the Coanda effect. The numerical results of differential static pressure obtained in CAS 21 and CAS 22 have the same appearance and are close to CAS 23. In perspective, numerical calculation in unsteady regime could be carried out to better understand the filling of the enclosure. The influence of the time constant of the heat source on the filling could be deepened by successively using sources of different diameters. The calculations could take into account the transfer by radiation.

Nomenclature

Lowercase:

l: Width Enclosure, m
x: Longitudinal coordinate, m
y: Vertical coordinate, m
z: Transverse coordinate, m
u: Horizontal component of the velocity, $m.s^{-1}$
v: Vertical component of the velocity, $m.s^{-1}$
w: Transverse velocity component, $m.s^{-1}$
w_0: Velocity along the (0z+) axis of the thermal plume at the surface of the heat source, m/s
cte: Constant
h_i: Heat exchange coefficient inside the enclosure, $W.m^{-1}.K^{-1}$
h_o: Heat exchange coefficient outside the enclosure, $W.m^{-1}.K^{-1}$
a: Thermal diffusivity
h: Convection heat transfer coefficient of the fluid out of the thermal plume, $W.m^{-1}.K^{-1}$

Capital Letters:

L: Enclosure length, m
H: Enclosure height, m
ΔT_0: Temperature difference in the thermal plume between the surface of the heat source and the ceiling of the enclosure, K
ΔT_1: Temperature difference between the thermal plume and the environment outside the plume at a given height z+, K
T: Temperature inside the enclosure, K
T_0: Temperature of the heat source, K
U_0: Maximum inlet gas velocity in the enclosure, K
P: Static pressure inside enclosure, Pa

P_{max}: Maximum static pressure inside enclosure, Pa
P_{total}: Total pressure, Pa
$P_{total,\ inside}$: Total pressure inside the enclosure, Pa
$P_{total,\ outside}$: Total pressure outside the enclosure, Pa
$T_{outside}$: Temperature outside the enclosure, K
T_p: Side wall or ceiling temperature, K
T_∞: Temperature away from side wall or ceiling inside or outside the enclosure, K
S_1: Section of the enclosure ceiling, m^2
S_2: Section of the side walls of the enclosure, m^2
S: External surface of the thermal plume, m^2
S_0: Base area of the thermal plume varying with enclosure height, m^2
C_P: Specific heat at constant pressure, J. $Kg^{-1}.K^{-1}$

Greek Symbols:

ν: Kinematic viscosity of air, $m^2.s^{-1}$
ρ: Density, $kg.m^{-3}$
ρ_0: Fluid density in thermal plume, $kg.m^{-3}$
β: Coefficient of thermal expansion, K^{-1}
ρ_{ext}: Density of gases outside of the enclosure, $kg.m^{-3}$
φ_p: Heat flux to the side walls and ceiling of the enclosure, $W.m^{-1}$
λ: Thermal conductivity of the walls in Plexiglas, $W.m^{-1}.K^{-1}$

Dimensionless Numbers:

Ra: Rayleigh number
Pr: Prandtl number
Gr: Grashof number

Special Characters:

Ra:* Reduced Rayleigh number
*Gr**: Reduced Grashof number
x+: Dimensionless longitudinal coordinate
y+: Dimensionless vertical coordinate
z+: Coordinated transverse to size
u+: Horizontal component of the dimensionless speed
v+: Vertical component of the dimensionless speed
w+: Transverse component of the dimensionless speed
P+: Static pressure to size
T+: Temperature to size
δ: Aspect Ratio

References

[1]. Le Masson S., Nortershauser D., Deddy B., Glouannec P. (2011) Thermal model for data centre cooling, Telecommunications Energy Conference (INTELEC), 33rd International IEE

[2]. Quintiere J. G. (2000) Enclosure Fire Dynamics, CRC Press LLC, Boca Raton USA

[3]. Quintiere, J. G., Rinkinen, W. J., Jones, W. W. (1981) Effect of Room Openings on Fire Plume Entrainment, Combustion Science and Technology, 26, 5-6, 193-201

[4]. Koueni Toko C. A. (2019), Etude des champs dynamique et thermique dans une enceinte semi – ventilée en convection naturelle, Rapport annuel de thèse – CORIA

[5]. Kouéni-Toko C. A., Tcheukam – Toko D., Kuitche A., Patte-Rouland B., Paranthoën P. (2020), Numerical modeling of the temperature fields in a semi-confined enclosure heated by a linear heat source, International Journal of Thermofluids, 100017. https://doi.org/10.1016/j.ijft.2020.100017

[6]. Kouéni Toko Christian Anicet (2022), Numerical Simulation of the Velocity Fields Generated by a Plume in Enclosure with Several Openings, International Journal of Fluid Mechanics & Thermal Sciences, 7(4), 53 – 67 doi: 10.11648/j.ijfmts.20210704.11

[7]. Kouéni – Toko Christian Anicet, Patte-Rouland Béatrice, Paranthoën Pierre. (2022), Experimental Study of the Pressure Generated by a Linear Heat Source in a Semi–ventilated Enclosure, Engineering and Applied Sciences, 7(1), 8 – 15 doi: 10.11648/j.eas.20220701.12

[8]. Koueni – Toko Christian Anicet (2022). Study of Thermal Fields in a Semi – Ventilated Enclosure Heated by a Linear Heat Source. International Journal of Fluid Mechanics & Thermal Sciences, 8(3), 53 – 63

[9]. Koueni, T. C. A. (2024). Natural Ventilation in a Semi-Confined Enclosure Heated by a Linear Heat Source. Transactions on Engineering and Computing Sciences, 12(1). 188-198.

[10]. Yu E., Yoshi Y. (1997) A numerical study of three-dimensional laminar natural convection in a vented enclosure, International Journal of Heat and Fluid Flow, 18, 6, 800-812

[11]. Jilani G., Jayaraj S., Khadar K. (2002) Numerical analysis of free convective flows in partially open enclosure, Heat and Mass Transfer, 38, 261-270

[12]. Desrayaud G., Lauriat G. (2004) A numerical study of natural convection in partially open enclosures with a conducting side-wall, J. Heat Transfer, 126, 1, 76-83

[13]. Miyamoto M., Kuehn T. H., Goldstein R.J., Katoh Y. (1989), Two-dimensional laminar natural convection heat transfer from a fully or partially open square cavity, Numerical Heat Transfer, Part A, 15, 4, 411-430

[14]. Prakash M., Kedare S. B., Nayak J. K. (2012) Numerical study of natural convection loss from open cavities, International Journal of Thermal Sciences, 51, 23-30

[15]. Baines W. D., Turner J. S. (1969) Turbulent buoyant convection from a source in a confined region, Journal of Fluid Mechanics, 37, 51-80

[16]. Morton B. R., Taylor G. I., Turner J. S. (1956), Turbulent gravitational convection from maintained and instantaneous sources, Proc. Roy. Soc. London, A, 234, 1 – 23

[17]. Patankar S. V. (1980), Numerical heat transfert and fluid flow, Hemisphere Publishing Corporation

[18]. Leonard, B. P. (1979), A stable and accurate convective 146odeling procedure based on quadratic interpolation, Comput methods Appl. Mech. Eng., 19, 59 – 98

[19]. Bouafia M., Daube O. (2007), Natural convection for large temperature gradients around a square solid body within a rectangular cavity, International Journal of Heat and Mass Transfer, 50, 3599 – 3615